Analyst

ROYAL SOCIETY
OF CHEMISTRY

PAPER
Marta Maria Natile, Niko Hildebrandt *et al.*
Er3+-to-dye energy transfer in DNA-coated core and
core/shell/shell upconverting nanoparticles with 980 nm
and 808 nm excitation of Yb3+ and Nd3+

Er³⁺-to-dye energy transfer in DNA-coated core and core/shell/shell upconverting nanoparticles with 980 nm and 808 nm excitation of Yb³⁺ and Nd³⁺†

Laura Francés-Soriano, [iD] ‡[a,b,c] Nicola Peruffo, [iD] §‡[d] Marta Maria Natile [iD] *[d] and Niko Hildebrandt [iD] *[a,b]

The capability of upconverting nanoparticles (UCNPs) to convert near infrared (NIR) into visible light has become an important feature for biosensing, imaging, therapy, and their combination. While significant achievements have been accomplished during the last decade developing nanohybrids based on UCNPs as energy donors in Förster resonance energy transfer (FRET) systems, it is still challenging to understand and control FRET from UCNPs to dyes and to adapt the NIR excitation wavelength. Here, we describe the synthesis, characterization, and steady-state and time-resolved FRET analysis of UCNP–DNA nanohybrids, in which dye labelled single stranded (ss)DNA was attached to Yb–Er-co-doped core UCNPs (c-UCNPs) and c-UCNPs with a thin Nd-doped shell and a second thin undoped shell (css-UCNPs). Despite differences in sizes, compositions, donor–acceptor distances, brightness, and excitation wavelength (980 nm for Yb³⁺ and 808 nm for Nd³⁺), all UCNP–DNA nanohybrids showed very similar concentration dependent FRET-quenching of UCNP luminescence with efficiencies between 0 and ~20%. We analyzed luminescence intensities, decay times, and rise times and could show the entanglement of excitation and emission kinetics by simply changing the excitation wavelength from 980 nm to 808 nm for the same css-UCNPs. Time-gated FRET-sensitized dye luminescence showed dye-ssDNA concentration dependence over four orders of magnitude (1 nM to 10 μM), which suggested a possible application to nucleic acid biosensing for both 808 and 980 nm excitation.

[a]Institute for Integrative Biology of the Cell (I2BC), Université Paris-Saclay, Université Paris-Sud, CNRS, CEA, 91405 Orsay Cedex, France.
E-mail: niko.hildebrandt@univ-rouen.fr
[b]nanoFRET.com, Laboratoire COBRA (Chimie Organique, Bioorganique, Réactivité et Analyse), Université de Rouen Normandie, CNRS, INSA, 76821 Mont-Saint-Aignan Cedex, France
[c]Instituto de Ciencia Molecular (ICMOL), University of Valencia, C/Catedrático José Beltrán, 2, Paterna, 46980, Spain
[d]Institute of Condensed Matter Chemistry and Technologies for Energy (ICMATE), National Research Council (CNR) and Department of Chemical Sciences, University of Padova, Via Francesco Marzolo 1, 35131 Padova PD, Italy.
E-mail: martamaria.natile@unipd.it
†Electronic supplementary information (ESI) available: XRD, TEM, TGA, DLS, hydrodynamic diameter, absorption and emission spectra, decay and rise times values, FRET efficiency. See DOI: 10.1039/c9an02532d
‡These authors have contributed equally. All authors have given approval to the final version of the manuscript.
§Present address: Department of Chemical Sciences, University of Padova, Via Francesco Marzolo 1, 35131 Padova, Italy.

Introduction

Förster resonance energy transfer (FRET) is a non-radiative energy transfer from an excited emissive donor (D) to an absorbing acceptor (A) molecule or nanoparticle through dipole–dipole interactions.[1,2] FRET is a direct and rapid method used in a wide range of applications such as biosensing, bioimaging or photodynamic therapy.[3–8] Efficient FRET requires two main prerequisites. First, the D–A pair should be located in close proximity, typically between 1 and 10 nm. Second, there needs to be a spectral match (energetic resonance) between the emission spectrum of the donor and the absorption spectrum of the acceptor.[9,10] FRET is also affected by the photoluminescence (PL) quantum yield (QY) of the donor, the molar extinction coefficients of the acceptor, the relative orientation of the transition dipole moments in the D–A pair, the refractive index of the surrounding medium, and the photostability of both donor and acceptor.

Upconverting nanoparticles (UCNPs) have attracted strong interest for their application as donors in FRET. UCNPs are a class of inorganic nanoparticles that are able to emit ultra-

violet (UV), visible (Vis), or near-infrared (NIR) light after absorbing NIR light, *i.e.*, they can generate upconversion luminescence (UCL).[11–15] They exhibit exceptional optical and chemical properties such as narrow emission bands, large anti-Stokes shifts, long PL lifetimes, resistance to photoblinking and photobleaching, and high thermo- and chemical stability.[16,17] NIR excitation allows for a deeper penetration into biological samples (*e.g.*, tissues) because of reduced light absorption and scattering compared to UV or Vis light.[14] Moreover, UCNPs possess almost negligible cytotoxicity.[18,19] Thus, UCNPs have become important PL agents for FRET-based sensing and imaging in biological applications.[20–22]

While energy transfer from/to quantum dots (considered as a point-dipole and following the FRET mechanism)[23] or to gold nanoparticles (considered as surface dipoles and following the nanosurface energy transfer mechanism – NSET)[24] have been extensively investigated and well understood, UCNP-based energy transfer is only in its infancy of comprehension. In UCNPs, every lanthanide ion emitter (activators, *e.g.*, Er^{3+} or Tm^{3+}) within the UCNP volume must be considered as a single donor and therefore, D–A distances (*e.g.*, with dyes on the UCNP surface) are very difficult to determine with high accuracy due to the following reasons: (i) Many activators inside the UCNP (close to the center) are too far away from a surface acceptors and only produce donor background PL, which makes it difficult to evaluate donor PL quenching for FRET analysis. (ii) The QY of the FRET donor is not the QY of the UCNP but the QY of each activator ion, which is very difficult to determine and may differ for the various activators. (iii) The many UCL-related energy transfer and energy migration steps (for both activators and sensitizers, *e.g.*, Yb^{3+} and Nd^{3+}) both populate and depopulate different non-emitting and emitting energy levels. (iv) In many cases, PL intensity and PL lifetime data do not provide the same results.[25–28] Owing to these difficulties, energy transfer processes involving UCNP donors are more intriguing to study because they cannot be simply predicted by conventional FRET theory. For example, Dukhno *et al.* have recently developed a semi-empirical Monte Carlo model for predicting the behavior of UCNP-dye systems.[29]

Despite the complicated dynamics, several studies have investigated the energy transfer processes for UCNPs, which were mainly related to FRET.[26–35] These studies used Yb/Er or Yb/Tm co-doped UCNPs and organic dyes (*e.g.*, BODIPY or rhodamine B) or other NPs (*e.g.*, quantum dots or perovskites) as acceptors. They demonstrated the critical role of the distribution of activators in the UCNPs, *i.e.*, only those ions close to the UCNP surface are able to undergo FRET to an acceptor attached to the surface. Therefore, the shell thickness, composition of core and/or shell, UCNP size, and even the organic capping are parameters to optimize in order to accomplish efficient FRET processes.

Nd^{3+}-doped UCNPs shift the excitation wavelength from 980 nm (Yb^{3+} excitation) to 808 nm, where the water absorption is around 0.02 cm^{-1}, more than 20 times lower than at 980 nm (0.482 cm^{-1}).[36] Moreover, the Nd^{3+} absorption cross-section ($\sim 1.2 \times 10^{-19}$ cm^2) is one order of magnitude higher than Yb^{3+}.[37]
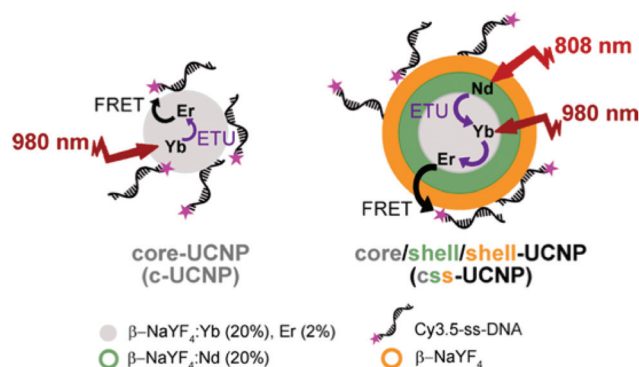
Consequently, the incorporation of Nd^{3+} ions into UCNPs can avoid water heating in long-term experiments, improve the light penetration depth, and increase the overall UCNP QY.[36] While such Nd^{3+}-sensitized UCNPs have become very interesting for *in vitro/in vivo* biological applications,[38] they have not been used to study FRET to dyes and compare the results to Yb^{3+}-sensitized UCNPs. Despite the enhanced properties mentioned above, UCNPs co-doped with Nd^{3+} as sensitizer and Er^{3+} or Tm^{3+} as activators display low QYs, owing to the energy back transfer from activators to Nd^{3+}.[39] To overcome this problem, researchers have developed multilayered structures and used Yb^{3+} as a bridge between Nd^{3+} and the activator ions. In such tri-doped nanostructures the Nd^{3+} ions harvest 808 nm light and transfers the energy to Yb^{3+}.[40,41] As a result, the Yb^{3+} ions are excited and able to transfer the energy to the activators (energy transfer upconversion – ETU). To accomplish high QYs, Nd^{3+} sensitizers and Er^{3+} (or Tm^{3+}) activators should be spatially separated along core and different shell structures, *i.e.* activators in the core and Nd^{3+} and Yb^{3+} sensitizers in the shell, suppressing the cross-relaxation process from activators to Nd^{3+}.[42]

In our present study, we have synthesized two different UCNP structures, namely "c-UCNP" and "css-UCNP" (Scheme 1). c-UCNP consisted of β-NaYF$_4$:Yb^{3+}(20%),Er^{3+}(2%) core, whereas css-UCNP was composed of a β-NaYF$_4$: Yb^{3+}(20%),Er^{3+}(2%)/NaYF$_4$:Nd^{3+}(20%)/NaYF$_4$ core/shell/shell structure. These UCNPs were further modified with a cyanine 3.5-labeled single-stranded DNA (Cy3.5-ssDNA) by anchoring it directly to positively charged UCNP surfaces through the numerous negatively charged phosphate groups in the DNA backbone. We studied the FRET processes from both UCNPs to Cy3.5 by steady-state and time-resolved luminescence spectroscopy with NIR irradiation at 980 nm and 808 nm and different Cy3.5-ssDNA concentrations.

Results and discussion

Synthesis and characterization of c-UCNPs and css-UCNPs

First, oleate-capped β-NaYF$_4$:Yb^{3+}(20%),Er^{3+}(2%) c-UCNPs and β-NaYF$_4$:Yb^{3+}(20%),Er^{3+}(2%)/NaYF$_4$:Nd^{3+}(20%)/NaYF$_4$

Scheme 1 Schematic representation of the two types of UCNPs and different energy transfer processes investigated in this study.

css-UCNPs with pure hexagonal phase structures were prepared, as confirmed by X-ray diffraction (XRD, Fig. S1(A)†). The c-UCNPs were obtained by the Ostwald ripening method following a modified procedure.[43] The css-UCNPs were synthesized following a layer-by-layer method employing sacrificial nanoparticles (s-UCNPs) as the shell precursor material.[44] These s-UCNPs (NaYF$_4$:Nd (20%) or NaYF$_4$) were produced by thermal decomposition methods and were found to be *ca.* 9 nm in diameter and of pure cubic α-phase (Fig. S1(B) and S2†). Once the β-NaYF$_4$:Yb^{3+}(20%),Er^{3+}(2%) c-UCNPs were formed, Nd-doped s-UCNPs were injected and allowed to ripen onto the surface of the c-UCNPs as an epitaxial, hexagonal-phase shell (300 °C, 15 min).[44] This process was repeated once more, using undoped α-NaYF$_4$ resulting in a second shell layer. The first (inner) layer contained the Nd^{3+} ions, which allowed for 808 nm excitation while keeping Nd^{3+} and Yb^{3+}/Er^{3+} ions separated (in shell and core, respectively) to mitigate energy back transfer from Er^{3+} to Nd^{3+}. The second (outer) layer consisted of an inert shell that minimized surface quenching effects, leading to brighter UCL.[45] Successful epitaxial shell growth on the c-UCNPs was corroborated by transmission electron microscopy (TEM, Fig. S3†). The average diameter of c-UCNPs (26 ± 2 nm) was increased to 28 ± 2 nm by addition of the Nd^{3+}-doped shell and to 31 ± 3 nm for the additional undoped shell. The size of c-UCNPs (different synthesis than for css-UCNPs) was 27 ± 2 nm (TEM, Fig. S4†). Both UCNPs were uniform in size and with a very small dispersion. The percentage of oleate on the UCNPs surface was determined by thermogravimetric analysis (TGA, Fig. S5†). The weight loss observed at ~450 °C was ~33% for s-UCNPs, 12% for c-UCNPs, and 11% for css-UCNPs. The lower amount of organic capping layer in c-UCNPs and css-UCNPs was caused by the higher surface-to-volume ratio of the s-UCNPs.

Both types of UCNPs showed the typical Er^{3+} emission bands (between 510 and 560 nm and between 640 and 680 nm) upon 980 nm and 808 nm excitation, respectively (Fig. 1). As expected, shell-coating of the c-UCNPs resulted in a

significant increase of the UCL brightness (13-fold) when the Yb^{3+} sensitizers inside the core (there is no Yb^{3+} inside the shells) were excited with 980 nm (red compared to black curve in Fig. 1). Excitation of css-UCNPs at 808 nm, *i.e.*, excitation of the Nd^{3+} sensitizers in the inner shell, resulted in ~14-fold lower UCL intensity compared to direct excitation of Yb^{3+} (980 nm) inside the core (blue compared to red curve in Fig. 1). This significantly lower intensity was also expected. While the absorption cross section of Nd^{3+} at 808 nm is higher and the water absorption at 808 nm is lower compared to Yb^{3+} and 980 nm (*vide supra*), the amount of Nd^{3+} ions in the ~1 nm thick inner shell is lower than the one of Yb^{3+} ions in the ~26 nm diameter core (4-fold lower when comparing the shell and core volumes and taking into account the equal doping ratio of 20% for both Yb^{3+} and Nd^{3+}). Moreover, the energy must be transferred from Nd^{3+} to Yb^{3+} and separation of Nd^{3+} (in the shell) and Er^{3+} (in the core) can only mitigate but not completely suppress energy backtransfer. More sophisticated multilayered UCNP structures are necessary to actually produce UCNPs that are brighter at 808 nm excitation compared to 980 nm excitation.[46–49]

DNA-conjugation of UCNPs

Considering that as prepared UCNPs were obtained with a hydrophobic oleate surface coating, a two-steps ligand exchange method was used to obtain hydrophilic ssDNA-conjugated UCNPs.

DNA possesses numerous negatively-charged phosphate groups, which can be attached *via* electrostatic interactions to the positively charged UCNPs. In the first step, oleate ligands were replaced with weakly bonded tetrafluoroborate anions (BF$_4^-$), by using the NOBF$_4$ protocol.[50,51] The second step consisted of the replacement of BF$_4^-$ anions with ssDNA (*cf.* Experimental section for details).[50] To study the efficiency of ssDNA coating and the stability of the prepared ssDNA–UCNP conjugates, different ssDNA : UCNP ratios were considered. Cy3.5-ssDNA allowed us to study both the stability of the ssDNA–UCNPs and UCNP-to-dye FRET under NIR irradiation as a function of Cy3.5-ssDNA concentration. Because attachment of Cy3.5-ssDNA to the UCNP surface was based on non-specific electrostatic interaction, the Cy3.5-ssDNA could adapt different orientations, possibly ranging from full DNA attachment (tangential to the UCNP surface) to full DNA extension (radial to the UCNP surface).[30] Such different DNA-surface assemblies influence both the stability of the UCNP-Cy3.5-ssDNA conjugates (the better the UCNP surface is covered the higher its stability in aqueous media) and the donor–acceptor distance (tangential orientation places the Cy3.5 acceptor close to the Er^{3+} donors, whereas radial orientation places it further away). To ensure both sufficient surface coating and close-enough donor–acceptor distance, we selected a ssDNA that was neither too short nor too long. The 20-nucleotide ssDNA used in our study should provide sufficient interaction with the UCNP surface and extend no more than 3 nm, when taking into account an extension of ~0.15 nm per nucleotide as previously found for ssDNA attached to quantum dot surfaces.[52]
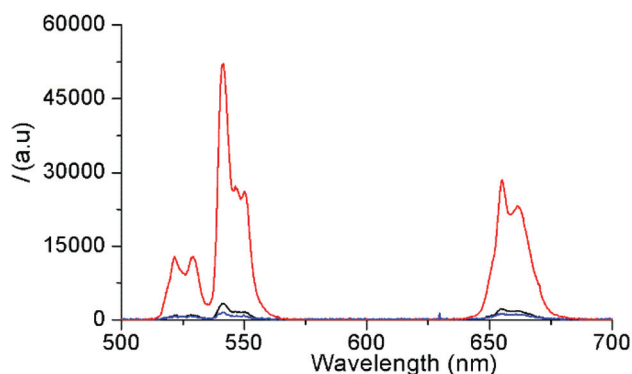

Fig. 1 PL intensity spectra of c-UCNP upon excitation at 980 nm (black), css-UCNP upon excitation at 980 nm (red), and css-UCNP upon excitation at 808 nm (blue). All UCNPs were conjugated with ssDNA and had a concentration of 10 mg mL^{-1} in water. The excitation power was constant for all PL spectra (P = 223 μW cm^{-2}).
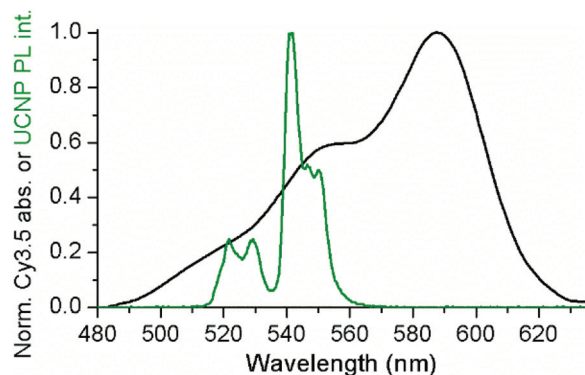
Fig. 2 The green PL bands of UCNPs (green) overlap with the absorption spectrum of Cy3.5 (black). See ESI† for calculation of overlap integrals.

With the resonance condition between UCNP donors and Cy3.5 acceptors being fulfilled, as shown by the spectral overlap between the green PL band of the UCNPs (λ_{exc} = 980 nm) and Cy3.5 absorption (Fig. 2), this maximum extension should provide favorable condition for a possible energy transfer. For both stability and FRET evaluation, the nominal Cy3.5-ssDNA : UCNP ratio was adjusted from *ca.* 0.1 to 4 nmol mg^{-1} using c-UCNPs.

The stability of an aqueous dispersion of DNA–c-UCNPs as a function of Cy3.5-ssDNA per c-UCNP ratio was evaluated by dynamic light scattering (DLS, Fig. S6†). Hydrodynamic diameters and polydispersity indices (PDI) were measured in triplicate for each sample and Table S1† displays the averaged values.

We noticed the formation of large aggregates for the ratios of 2.0 and 2.5 nmol mg^{-1}, with average sizes above 500 nm. Below 2.0 nmol mg^{-1}, the amount of ssDNA was not sufficient to favor aggregation. For higher Cy3.5-ssDNA per c-UCNP ratios (4.0 nmol mg^{-1}) nanohybrids displayed a better stability in water over time and no size changes were observed even after several measurement, which we ascribed to an efficient UCNP surface coating with DNA.

The optical properties of Cy3.5 and c-UCNP as a function of Cy3.5-ssDNA per c-UCNP ratio were investigated by absorption and PL spectroscopy. Probing Cy3.5 resulted in increasing intensities (with increasing Cy3.5-ssDNA per c-UCNP ratio) for absorption (Fig. S7†), PL emission (Fig. S8†), and PL excitation (Fig. S9†), as expected due to the increasing Cy3.5 concentration. Upon NIR-excitation of UCNPs, the PL decay curves of both the green Er^{3+} PL of UCNPs (Fig. 3A) and the red PL of Cy3.5 (Fig. 3B) showed the characteristic rise and decay profiles of UCNPs, which extend over a few hundred microseconds. Taking into account that Cy3.5 cannot be excited at 980 nm and that the PL decay of Cy3.5 is in the nanosecond range, the long PL decay of Cy3.5 provided clear evidence of dye-sensitization *via* FRET from UCNPs.

The intensities of the time-resolved PL curves also confirmed the stability results obtained with DLS (*vide supra*). Increasing amounts of Cy3.5-ssDNA clearly improved the
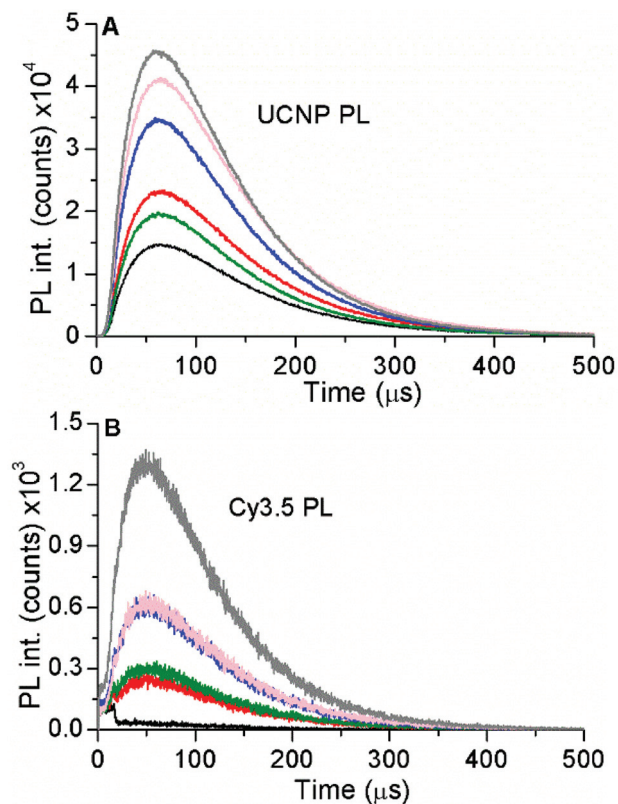

Fig. 3 Time-resolved PL intensities of c-UCNPs (A, λ_{em} = 542 ± 10 nm) and Cy3.5 (B, λ_{em} = 607 ± 5 nm) for different ratios of Cy3.5-ssDNA per c-UCNP (0.09 nmol mg^{-1} – black; 0.47 nmol mg^{-1} – red; 0.97 nmol mg^{-1} – green; 1.89 nmol mg^{-1} – blue; 2.46 nmol mg^{-1} – pink; 3.54 nmol mg^{-1} – gray) in water upon excitation at 980 nm. The concentration of c-UCNPs was constant (1 mg mL^{-1}).

UCNP PL (higher intensities), which also resulted in higher UCNP-sensitized Cy3.5 PL intensities. Interestingly, the Cy3.5 PL intensity increase did not follow the same trend as the UCNP PL intensity. For the lowest Cy3.5-ssDNA per c-UCNP ratio (0.1 nmol mg^{-1}), Cy3.5-sensitization was negligible, most probably caused by the low Cy3.5 concentrations, which also resulted in very low Cy3.5 absorption (Fig. S7†) and emission upon direct Cy3.5 excitation (Fig. S8†). The higher ratios (0.5 to 2.5 nmol mg^{-1}) showed significant Cy3.5 sensitization but without a ratio-specific intensity increase (as found for UCNP PL), which can be ascribed to the reduced stability of the Cy3.5-ssDNA–c-UCNP conjugates at these conjugation ratios. Similar to DLS, the best results (highest intensities for both UCNP and Cy3.5 PL) were found for the nominal ratio of 4 nmol Cy3.5-ssDNA per mg c-UCNP and we used this conjugation condition for the following FRET investigations with both c-UCNPs and css-UCNPs.

FRET studies

For maintaining a constant amount of DNA on the UCNP surface (3.54 nmol DNA per mg UCNP), we used both Cy3.5-ssDNA and unmodified ssDNA. The concentrations of Cy3.5-ssDNA in the synthesis mixture was increased from 0 to 4 μM

(0, 0.001, 0.01, 0.05, 0.1, 0.5, 1.0, 2.0, 3.0, and 4.0 µM) while the amount of ssDNA was decreased from 4 to 0 µM. The UCNP concentration was kept constant at 1 mg mL^{-1}. To obtain sufficient PL intensity for steady-state spectroscopy analysis (*vide infra*), all concentrations were 10-fold higher but DNA per UCNP ratios were the same.

First, DLS and ζ-potential measurements were performed on c-UCNPs and css-UCNPs capped entirely with Cy3.5-ssDNA and ssDNA, respectively. This approach allowed us to obtain information about the effect of the dye on the stability of UCNP–DNA conjugates. It is noteworthy that the hydrodynamic diameters of UCNP–Cy3.5-ssDNA conjugates were significantly smaller than those of UCNP–ssDNA (*e.g.*, ~136 nm *vs.* ~176 nm, Table S2†). While this is somewhat counterintuitive, it may be caused by dye-related changes in the hydration layer rather than a reduced size. The ζ-potentials (Table S2†) of all UCNP–ssDNA conjugates (with and without Cy3.5) were negative (between *ca.* −4 and −13 mV) and there was no significant difference between ssDNA and Cy3.5-ssDNA. Considering the positive surface charge (ζ-potential of +23.3 mV) of the BF$_4$-coated UCNPs, the negative values provided good evidence that ssDNA (with and without Cy3.5), with its numerous negatively charged phosphate groups, was successfully attached to the UCNP surfaces.

We first used steady-state PL spectroscopy to analyze DNA-mediated FRET from UCNP to Cy3.5 for different conjugates of c-UCNP-Cy3.5-ssDNA/ssDNA and css-UCNP-Cy3.5-ssDNA/ssDNA upon excitation at 980 and 808 nm (Fig. S10 and S11†). Importantly, the cores of c-UCNPs and css-UCNPs contained almost an equivalent amount of sensitizer and activator ions. Therefore, differences between the samples' optical properties could be ascribed to the two shells in the css-UCNPs. Under 980 nm excitation, Yb^{3+} and Er^{3+} co-doped materials undergo UCL mainly *via* ETU. Yb^{3+} ions absorb NIR light ($^2F_{7/2} \rightarrow {}^2F_{5/2}$) and, subsequently transfer the energy to emitting Er^{3+} excited states involving a two or three photon processes.

The radiative deactivation of these Er^{3+} excited states results in three main emission bands at *ca.* 520 nm ($^2H_{11/2} \rightarrow {}^4I_{15/2}$), 540 nm ($^4S_{3/2} \rightarrow {}^4I_{15/2}$), and 660 nm ($^4F_{9/2} \rightarrow {}^4I_{15/2}$).[53] Excitation at 808 nm adds an additional energy transfer step from Nd^{3+} to Yb^{3+}. Nd^{3+} is excited from the $^4I_{9/2}$ to $^4F_{5/2}$ state, relaxes non-radiatively to the $^4F_{3/2}$ level through multiphonon processes and then energy is transferred to nearby Yb^{3+} ions in the NPs core, exciting them to the $^2F_{5/2}$ state.

For all UCNP–DNA nanohybrids, Cy3.5-ssDNA concentration dependent UCL quenching of the green PL bands (510–560 nm) of Er^{3+} could be clearly observed. Because the red PL band (640–675 nm) did not overlap with Cy3.5 absorption (no energetic resonance) but is sensitive to small sample-related intensity fluctuations, the green-to-red UCL intensity ratio (I_{540}/I_{660}) was used to analyze the Cy3.5-ssDNA concentration dependence of FRET quenching. While the green-to-red UCL ratio was higher for css-UCNP[λ_{ex} = 980 nm] (most probably due to the more than 10-fold brighter UCL – *cf.* Fig. 1), the relative quenching was very similar for all UCNP–DNA conjugates (Fig. 4 and Fig. S12, S13†).
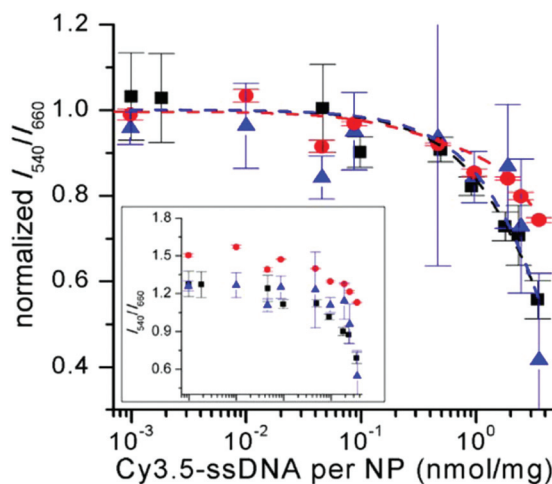

Fig. 4 Cy3.5-ssDNA concentration dependent PL intensity ratios (I_{540}/I_{660} – normalized to unity for samples without Cy3.5-ssDNA) of c-UCNP (black) and css-UCNP (red) upon excitation at 980 nm and of css-UCNP upon 808 nm excitation (blue). The inset shows the non-normalized data (abscissa has the same scale than the normalized graph – larger version of the inset can be found in Fig. S13†). PL intensities were integrated over the entire green and red PL bands (510 to 560 nm for I_{540} and 640 to 675 nm for I_{660}).

The much stronger UCL signal of css-UCNP[λ_{ex} = 980 nm] also resulted in more precise measurements (error bars of css-UCNP[λ_{ex} = 808 nm] and c-UCNP[λ_{ex} = 980 nm] are significantly larger – *cf.* Fig. 4).

Low concentrations of Cy3.5-ssDNA (below ~0.1 nmol mg^{-1}, which corresponds to ~1/40 Cy3.5-ssDNA/ssDNA or ~100 Cy3.5-ssDNA per UCNP) did not result in significant UCL quenching, whereas full coverage of UCNPs with Cy3.5-ssDNA led to quenching between ~25% for css-UCNP[λ_{ex} = 980 nm] and ~55% for css-UCNP[λ_{ex} = 808 nm].

Taking into account that the signals of c-UCNP and css-UCNP[λ_{ex} = 808 nm] were even lower when FRET-quenched, the css-UCNP[λ_{ex} = 980 nm] data was quantitatively the most reliable, whereas the other two UCNP–DNA nanohybrids confirmed the clear trend of Cy3.5-ssDNA concentration dependent quenching. This assessment of similar FRET-quenching for all UCNP–DNA conjugates (despite their differences in D–A distances and excitation wavelengths) with a maximum efficiency around 20% was also confirmed by time-resolved measurements (*vide infra*).

While UCL quenching was obvious, we could unfortunately not observe significant FRET-sensitized Cy3.5 PL. One reason was the lacking sensitivity of our steady-state spectroscopy setup (fibre-coupled CCD spectrometer), which required the use of relatively high UCNP–DNA concentrations (10 mg mL^{-1}, *vide supra*). More importantly, the relatively high concentration of the dye increased the probability of the formation of non-fluorescent H-aggregates, which acted as trap states for both FRET from UCNPs or homo-FRET from other dyes. Such trap states at high concentrations of dyes on nanoparticles can lead to strong self-quenching of the fluorescence.[54] The formation
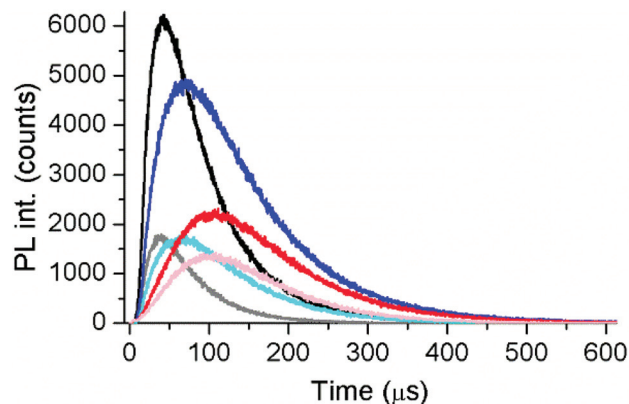
Fig. 5 Time-resolved PL intensities (λ_{em} = 542 ± 10 nm) of UCNP–DNA nanohybrids without (no FRET) and with (FRET) 3.54 nmol mg^{-1} Cy3.5-ssDNA. Black/gray: c-UCNP–DNA without/with Cy3.5-ssDNA (λ_{ex} = 980 nm); blue/cyan: css-UCNP–DNA without/with Cy3.5-ssDNA (λ_{ex} = 980 nm); red/rose: css-UCNP–DNA without/with Cy3.5-ssDNA (λ_{ex} = 808 nm).

Fig. 6 Cy3.5-ssDNA concentration dependent PL decay time ratios of quenched (τ_{DA}) and unquenched (τ_D – no Cy3.5-ssDNA) c-UCNPs (black) and css-UCNPs (red) upon excitation at 980 nm and of css-UCNPs upon 808 nm excitation (blue). Inset shows the same ratios as a function of amount (copies) of Cy3.5-ssDNA per NP.

of H-aggregates was confirmed by UV-Vis absorption spectra of nanohybrids with different amounts of Cy3.5-ssDNA (Fig. S7†) even at low concentrations of UCNP–DNA nanohybrids (1 mg mL^{-1}). These spectra showed a more intense blue absorption shoulder (around 550 nm) compared to non-aggregated dyes (Fig. 2), which is typical for H-aggregates.[55–57]

To gain further insight into the energy transfer processes, we carried out time-resolved PL measurements with filter-based photomultiplier detection. This allowed us to analyze the decay times of both FRET-quenched UCL and FRET-sensitized Cy3.5 fluorescence (Table S3†) and the rise times of FRET-quenched UCL (Table S4†) for all UCNP–DNA nanohybrids. Moreover, we could use a UCNP–DNA concentration of 1 mg mL^{-1}. For a direct comparison with the steady-state data, we first analyzed the green emission (~540 nm) of c-UCNPs and css-UCNPs upon 980 and 808 nm excitation (Fig. 5 and Fig. S14†). Consistent with the steady-state PL results (Fig. 4), increasing concentrations of Cy3.5-ssDNA per UCNP resulted in increased UCL decay time quenching, which was similar for all UCNP–DNA conjugates (Fig. 6).

The more sensitive detection setup and the independence of PL lifetime from sample concentration resulted in significantly less deviations compared to the steady-state measurements.

They also confirmed our assessment that the Cy3.5-ssDNA concentration dependent FRET quenching is the same for all UCNPs, almost negligible for low Cy3.5-ssDNA concentrations (although the more sensitive setup leads to an onset of FRET quenching at slightly lower concentrations), and reaches a maximum of approximately 20% at coverage of UCNPs with only Cy3.5-ssDNA (Fig. 6).

Owing to the smaller size of the c-UCNPs, their molar concentration is higher compared to the css-UCNPs (for the same weight of 1 mg). Therefore, UCL quenching as a function of copies (molecules) of Cy3.5-ssDNA (Fig. 6 inset) results in
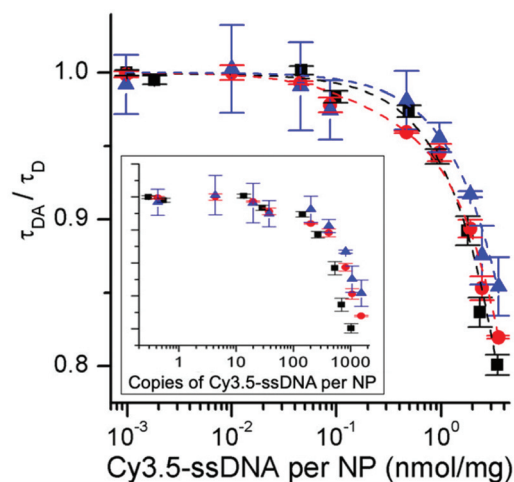
slightly less Cy3.5-ssDNA for the same quenching efficiencies when comparing c-UCNPs and css-UCNPs. This finding makes sense because the c-UCNP size is smaller and the D–A distance is shorter (no shell).

The different UCNPs and excitation wavelengths also resulted in different absolute decay times (Fig. 7A). c-UCNPs had the shortest decays because of direct contact of the Er^{3+} emitters with the environment, which was avoided in the shelled css-UCNPs. The shorter decay times of css-UCNP[λ_{ex} = 808 nm] compared to css-UCNP[λ_{ex} = 980 nm] were less intuitive because only the excitation wavelengths were different, whereas the UCNPs were exactly the same.

This finding reflects the direct relation between excitation and emission in UCNPs, which is caused by the many long-lived excited states and many possible pathways of both excitation and deexcitation. The UCL rise times confirmed the differences (Fig. 7B). c-UCNPs were deactivated very quickly ($\tau_D \sim$ 60 µs) and therefore the emissive excited state cannot be populated for a very long time (relatively short rise time of
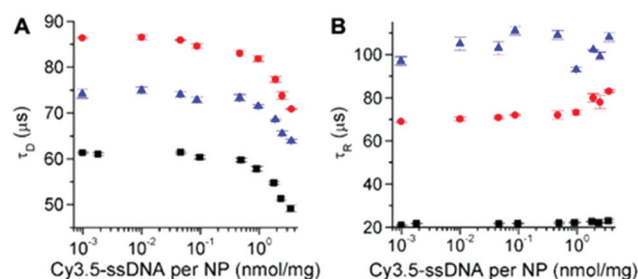
Fig. 7 UCL decay (A) and rise (B) times of c-UCNPs (black) and css-UCNPs (red) upon excitation at 980 nm and of css-UCNPs upon 808 nm excitation (blue) as a function of Cy3.5-ssDNA concentration.

$\tau_R \sim 20\ \mu s$). The well-protected Er^{3+} emitters in the css-UCNPs were deactivated more slowly ($\tau_D \sim 85\ \mu s$) and thus, population of the emissive excited state could become longer ($\tau_R \sim 70\ \mu s$). On the other hand, excitation of the emissive state *via* additional pathways from Nd^{3+} to Yb^{3+} was slower ($\tau_R \sim 100\ \mu s$). This slower excitation could also be the reason for the quicker deactivation ($\tau_D \sim 75\ \mu s$) because there is less excitation during deactivation. While these considerations only provide a very simplistic view, the differences in both decay and rise times, even for the same UCNPs that were excited at different wavelengths/activators, clearly showed the entanglement of excitation and deactivation pathways in UCNPs. The Cy3.5-ssDNA concentration dependence of both decay and rise times (decay times decrease and rise times slightly increase at high Cy3.5-ssDNA concentrations) is another indicator that the additional FRET pathway influences both excitation and deactivation of UCNPs. More detailed investigations, which were out of the scope of our present study, will be necessary to obtain a better understanding of the relation between FRET and UCNP excitation and deactivation.

The time-resolved spectroscopy setup was also able to detect sufficient FRET-sensitized Cy3.5 fluorescence around 607 nm (Fig. S15†), which allowed us to analyze FRET-sensitized decay times (Table S3†), whereas the signals were unfortunately too weak to adequately fit rise times. For low Cy3.5-ssDNA concentrations (below $\sim 0.1\ nmol\ mg^{-1}$), FRET-sensitized fluorescence (in the μs range) was only weakly above background levels and decay times could not be determined. This was in agreement with both steady-state and time-resolved UCL quenching, which did not show significant FRET at low concentrations either. For higher concentrations, the decay times were very similar to those found for UCL-quenching.

Taking into account that the intrinsic fluorescence lifetime of Cy3.5 is in the order of nanoseconds, this long decay time transition from UCNP to Cy3.5 clearly confirmed that the Cy3.5 excitation energy was provided by FRET from the long-lived excited states of Er^{3+}. Interestingly, the time-gated intensities (integrated intensities from 20 μs to 300 μs in the Cy3.5 decay curves) increased with increasing Cy3.5-ssDNA concentrations over approximately four orders of magnitude (Fig. S16†) for both c-UCNP–DNA and css-UCNP–DNA nanohybrids. Although the aim of our study was not the development of DNA biosensors, the DNA concentration dependence of these systems (at both 980 and 808 nm) showed that they could in principle be used for DNA sensing.

Experimental

Materials and methods

Materials. Y_2O_3 (99.9%), Yb_2O_3 (99.9%), Er_2O_3 (99.99%) and Nd_2O_3 (99.9%) were purchased from Alfa Aesar. Hydrochloric acid (37%), sodium trifluoroacetate (Na(CF$_3$COO), 98%), ammonium fluoride (NH$_4$F, 98%), sodium hydroxide (NaOH,

97%), 1-octadecene (ODE, 90%), oleic acid (OA, 90%), *N*,*N*-dimethylformamide (DMF, 99.8%), nitrosonium tetrafluoroborate (NOBF$_4$, 69.9–78.8%), ethanol (EtOH, 99.8%), toluene (99.9%), chloroform (CHCl$_3$, 99.8%) and trifluoroacetic acid (CF$_3$COOH, 99%) were all obtained from Sigma-Aldrich. Methanol (99.9%) was purchased from Romil Pure Chemistry. *N*-Hexane (97%) was from VWR Chemicals. Dichloromethane (CH$_2$Cl$_2$, 99.9%) was from R.P. Normapur. Cyclohexane (99%) was purchased from Acros Organics. All chemicals were used as received without further purifications. Highly pure water (Millipore) of resistivity greater than 18.0 $M\Omega$ cm was used in all experiments, except in those involving DNA where free-RNA water was used. DNA strands were purchased from Eurogentec. The ssDNA sequence was AAT CAA GGT AAC GGA CTG AG. Two kinds of ssDNA were used: unlabeled ssDNA and ssDNA labeled on the first base with a cyanine 3.5 (Cy3.5-AAT CAA GGT AAC GGA CTG AG).

Powder X-ray diffraction (PXRD). PXRD measurements were carried out with a Bruker D8 Advance diffractometer using Cu Kα radiation (λ = 1.5406 Å) at a voltage of 40 kV and current of 40 mA. PXRD patterns were collected for 2θ = 10–70°, with a step size of 0.03° and a counting time of 10 s per step. The crystalline phases were identified by the search-match method using the JCPDS database. Before each measurement 20 mg of the sample were dried under vacuum.

Transmission electron microscopy (TEM). TEM samples were prepared by drop casting ($\sim$50 μL) of an oleate capped UCNPs dispersion in toluene (1 mg mL^{-1}) onto 400-mesh carbon-coated Cu grids, followed by air-drying. TEM images were taken on a FEI Tecnai G2 TEM operating at 100 kV, equipped with an Olympus Veleta camera. The Fiji ImageJ software was used to determine the UCNPs size, which was obtained as the average diameter of 200 individual nanoparticles. For each css sample, core and core–shell intermediates were also analyzed by TEM in order to determine the shell thickness.

TGA. TGA was carried out using the SDT 2960 Simultaneous DSC-TGA system (TA Instruments). 15 mg of dried powder was heated from 25 °C to 700 °C, with an increase of 10 °C min^{-1} under nitrogen flow.

DLS and ζ-potential. A Zetasizer Nano ZS was used. UCNPs dispersions in water (0.01 mg mL^{-1}) were prepared by sonication for 20 min and then were placed in disposable polystyrene cuvettes. The instrument was equipped with a 532 nm laser and a detector in configuration NIBS (non-invasive backscatter system – 173°). The temperature was kept at 25 °C during the measurement. The measurements were made by triplicate. Zetasizer software was used to analyze the data.

UV-Vis characterization. A single beam PerkinElmer Lambda 35 spectrophotometer was used to perform all the absorbance measurements. The bandwidth was 1 nm, the measured region from 200 nm to 800 nm. Before each measurement session, 100% and 0% transmittance spectra were required from the software. 80 μL of each sample dispersion were placed in a (1 cm × 150 μm) cuvette to be analyzed. The concentration of the UCNPs was 1 mg mL^{-1}.

Fluorescence measurements. For the dye emission and excitation spectra a SAFAS Xenius spectrofluorometer was used. 100 μL of UCNPs dispersion (1 mg mL^{-1}) were placed in a 96-well microplate. All the measurements were carried out with a bandwidth of 2 nm, a photomultiplier voltage of 1050 V and an integration time of 0.1 s. To obtain the UCNPs time-resolved measurements, a fluorescence plate reader from Edinburgh Instruments equipped with 2 W 980 nm and 2 W 808 nm lasers (Changchun New Industries) and a PM-1 laser modulation box (Edinburgh Instruments) for controlling the pulsing parameters was used. To focalize the laser beam into the samples, 750 nm and 900 nm dichroic filters (Edmund Optics Inc) were used for the 808 and 980 nm laser, respectively. The decay curves were collected in a PMT using the appropriate bandpass filters (Semrock) of 542/20 nm for the UCNPs green band, 660/13 nm for the UCNPs red band and 607/10 nm for the dye. The UCNPs concentration was 1 mg mL^{-1}. UCNP steady-state PL spectra and steady-state FRET analysis were obtained using a fibre coupled CCD-spectrometer and SpectraSuite software (Ocean Optics). Due to the lower sensitivity of this setup, the used UCNP–DNA concentrations were 10-fold higher (10 mg mL^{-1}). ssDNA and Cy3.5-ssDNA concentrations were also 10-fold higher to obtain the same ssDNA per UCNP ratios as for time-resolved detection.

Synthetic procedures

Synthesis of oleate-capped β-NaYF$_4$:Yb^{3+}(20%),Er^{3+}(2%) nanoparticles (c-UCNPs). The synthesis of β-NaYF$_4$:Yb^{3+}(20%), Er^{3+}(2%) UCNPs was carried out by a modified literature procedure.[43] Rare earth chloride precursors were prepared from the rare earth oxides. Briefly, Y$_2$O$_3$ (0.78 mmol), Yb$_2$O$_3$ (0.20 mmol), and Er$_2$O$_3$ (0.02 mmol) were dissolved in 4.2 mL of 1.7 M HCl aqueous solution in a three neck round bottom flask. The solution was stirred under reflux at 80 °C until the solution became clear (overnight). Then, the solvent was removed by evaporation at 65 °C. The powder was dried further in the oven at 105 °C. At this point 6 mL of OA and 15 mL of ODE were added under Ar flow to the previously obtained precursors. The mixture was heated at 150 °C under vacuum and magnetic stirring until the precursors were dissolved. The reaction mixture was cooled down to room temperature under Ar flow and then, 10 mL of a methanol solution containing NaOH (2.5 mmol) and NHF$_4$ (4.0 mmol) was added drop by drop. Subsequently, the solution was slowly heated under argon flow and magnetic stirring until 120 °C to remove the methanol and then heated at 300 °C and kept at this temperature for 70 min. Then, the solution was cooled down to room temperature under argon flow and the nanoparticles were precipitated from the solution with ethanol (~40 ml) and collected by centrifugation (4000 rpm for 15 min). The resulting white pellet was further washed four times with a mixture of hexane/ethanol (1 : 3) and isolated by centrifugation (4000 rpm, 15 min). Finally, the white pellet was stored in ethanol.

Sacrificial nanoparticles (s-UCNPs) synthesis. Two s-UCNPs were synthesized: α-NaYF$_4$ and α-NaYF$_4$:Nd^{3+}(20%). First, Y(CF$_3$COO)$_3$ and Nd(CF$_3$COO)$_3$ precursors were prepared from the Y$_2$O$_3$ and Nd$_2$O$_3$. Briefly, 2 mmol of a Y$_2$O$_3$ (or a stoichiometric mixture of Y$_2$O$_3$ and Nd$_2$O$_3$) were placed in a three necks bottom round flask. Then, 5 mL of milliQ water and 5 mL of trifluoroacetic acid (TFA) were added and the mixture was stirred under reflux at 80 °C overnight. When the solution was clear, the excess of water and TFA was removed by evaporation at 65 °C in air. The obtained powder was dried in the oven at 105 °C. Next, 2 mmol of sodium trifluoroacetate (NaTFA) was added to the precursors' flask. Then, 6 mL of OA, 6 mL of oleylamine (OM) and 10 mL of ODE were added under Ar flow. This mixture was heated at 125 °C in vacuum atmosphere under vigorous stirring. After that, the reaction was heated at 290 °C in argon atmosphere for 45 min. Then, the reaction was cooled to room temperature. The sacrificial nanoparticles were precipitated by addition of ethanol and isolated by centrifugation (4000 rpm, 15 min). The obtained precipitate was washed twice as reported for c-UCNPs. Finally, nanoparticles were dispersed in ODE (0.3 mM).

Synthesis of oleate-capped β-NaYF$_4$:Yb^{3+}(20%),Er^{3+}(2%)/ NaYF$_4$:Nd^{3+}(20%)/NaYF$_4$ (css-UCNPs). The synthesis of core–shell–shell UCNPs (css-UCNPs) was based on a previously described protocol.[44] First, the β-NaYF$_4$:Yb^{3+}(20%),Er^{3+}(2%) core was synthesized as previously described above for c-UCNPs. After heating the reaction mixture at 300 °C for 70 min, 1 mL aliquot was collected. Immediately after that, 1 mL of α-NaYF$_4$:Nd^{3+}(20%) 0.3 mM dispersion in ODE was injected in one shot. Next, this mixture was heated at 300 °C for 15 min to allow the growth of the NaYF$_4$:Nd^{3+}(20%) shell around the core nanoparticles. Then, 1 mL of the reaction mixture was retrieved and 1 mL of α-NaYF$_4$ dispersion in ODE (0.3 mM) was injected in one shot. The reaction was heated again at 300 °C for 15 min to lead oleate-capped β-NaYF$_4$: Yb^{3+}(20%),Er^{3+}(2%)/NaYF$_4$:Nd(20%)/NaYF$_4$ nanoparticles (css-UCNPs). The solution was cooled down to room temperature and the css-UCNPs were precipitated by addition of ethanol and centrifugation (4000 rpm, 15 min). The white precipitate was washed as described for c-UCNPs. Finally, nanoparticles were stored under ethanol.

Surface modification of UCNPs with DNA. First, the OA ligands were replaced by BF$_4^-$ following a described procedure.[51] Briefly, 10 mg of UCNPs were transferred in a centrifuge tube (15 mL) and 2 mL of cyclohexane were added (≈5 mg mL^{-1}). The mixture was sonicated until complete UCNPs redispersion (~30 minutes). Next, 2 mL of a 0.01 M solution of NOBF$_4$ in DCM/DMF (30 : 1) were added. The dispersion was stirred in a vortex for 30 s. Then, UCNPs-BF$_4$ were recovered by centrifugation (15 min, 4300 rpm, RT). The precipitate was sonicated twice with 2.2 mL of a toluene : hexane mixture (1 : 1 by volume) for 15 minutes and then, centrifuged again (15 min, 4300 rpm, RT). The colorless pellet was stored in 1 mL of DMF (10 mg mL^{-1}), ready for the successive ligand exchange. Then, 0.1 mL of the UCNPs-BF$_4$ in DMF (1 mg UCNPs) dispersion were transferred in a 2 mL Eppendorf tube and the desired amount of Cy3.5-ssDNA was added to the solution. The Cy3.5-ssDNA : UCNPs nominal ratios were 0.1, 0.5, 1,

Table 1 Comparison of other UCNP-dye FRET systems with the results obtained in the present study(*). SS: steady-state PL measurements, TR: time-resolved PL measurements

UCNPs			Quenching (%)		
Composition	Size (nm)	Dye	SS	TR	Ref.
$NaYF_4$:Yb,Er	27 ± 2	Cy3.5	20	20	*
$NaYF_4$:Yb,Er@$NaYF_4$:Nd@$NaYF_4$	31 ± 3	Cy3.5	20	20	*
$NaYF_4$:Yb,Er@$NaYF_4$	27.4	Rose bengal	30	50	31
$NaYF_4$:Yb,Er	38.4 ± 1.7	BODIPY	50	19	26
$NaYF_4$:Yb,Er	20	Rose bengal	83	40	27
$NaYF_4$:Yb,Er,Tm	23.1 ± 1.1	Napthalimide and porphyrin	80	50	58
$NaYF_4$:Yb,Er	10 to 43	Rose bengal Sulforhodamine B	—	10 to 55	28
$NaYF_4$:Yb,Er@$NaYF_4$	10 to 43	Rose bengal Sulforhodamine B	—	10 to 60	28
$NaYF_4$:Yb,Er	30.6 ± 1.1	Rhodamine B	20	10	29
$NaGdF_4$:Yb,Er	17 ± 2	Cy3.5	—	49	30
$NaGdF_4$:Yb,Er@$NaGdF_4$	24 ± 3	Cy3.5	—	25	30
$NaGdF_4$@$NaGdF_4$:Yb,Er	15 ± 3	Cy3.5	—	45	30
$NaYF_4$:Yb,Tm	6.3	DBD-6	—	30	59
$NaYF_4$:Yb,Tm@$NaYF_4$	5.5	DBD-6	—	15	59
$NaYF_4$:Yb,Er@$NaYF_4$	26 to 44	Rose bengal	10 to 20	—	60

2, 2.5 and 4 nmol mg^{-1}. Next, RNA-free water was added up to 1 mL of total volume. The dispersion was stirred in an orbital shaker (600 rpm, 3 hours, RT) and finally incubated overnight at 4 °C. After that, the reaction mixture was centrifuged (12 min, 12 000 rpm, RT) and the pellet was redispersed in 1 mL of RNA-free water, sonicated for 20 min and centrifuged again (12 min, 12 000 rpm, RT). The washing cycle sonication/centrifugation was repeated three times in total (3 mL of water). The purified Cy3.5-ssDNA–UCNPs were redispersed in 1 mL of RNA-free water (1 mg mL^{-1}) and stored at 4 °C for further experiments. The final amounts of the ssDNA-Cy3.5 on the UCNPs surface were determined by absorbance measurements and were 0.09 nmol mg^{-1}, 0.47 nmol mg^{-1}, 0.97 nmol mg^{-1}, 1.89 nmol mg^{-1}, 2.46 nmol mg^{-1}, 3.54 nmol mg^{-1}, respectively.

Conclusions

FRET with UCNPs and modification of the UCNP excitation wavelength from 980 nm to 808 nm by using Nd^{3+} activators instead of Yb^{3+} are two important topics in the development of UCNP-based biosensors and imaging agents. However, combining FRET and Yb^{3+}/Nd^{3+} co-doping in UCNPs to gain a more profound understanding of UCNP-to-dye FRET and to use this understanding for better biosensor development has not been investigated. With the aim to learn more about UCNP-based FRET and to possibly apply this knowledge for future UCNP-FRET biosensors, we synthesized Yb^{3+}/Er^{3+} co-doped UCNPs and coated them with a thin Nd^{3+}-doped shell and a second undoped shell to yield comparable Yb^{3+}/Er^{3+}-core UCNPs (c-UCNP) and Yb^{3+}/Er^{3+}-core/Nd^{3+}-shell/protective-shell UCNPs (css-UCNPs).

Owing to the same core for both UCNPs, they differed only in their brightness (css-UCNPs were protected from the environment by the outer undoped shell) and the possible excitation wavelength (in c-UCNPs only Yb^{3+} could be excited by 980 nm whereas in css-UCNPs Yb^{3+} in the core could be excited by 980 nm and Nd^{3+} in the inner shell could be excited by 808 nm). The higher brightness was experimentally confirmed by a ~13-fold increase from c-UCNP[λ_{ex} = 980 nm] to css-UCNP[λ_{ex} = 980 nm]. Although the shell contained only ~4 times less Nd-ions than Yb-ions in the core, css-UCNP[λ_{ex} = 808 nm] were ~14-fold less bright than css-UCNP[λ_{ex} = 980 nm]. Despite the lower water absorption at 808 nm and the higher absorption cross section of Nd^{3+} compared to Yb^{3+}, the decreased brightness was most probably caused by energy backtransfer from Er^{3+} to Nd^{3+} at the core–shell interface, and showed that more sophisticated core/shell architectures are necessary for fully exploiting the advantageous properties of Nd^{3+} activators.

More important than the somewhat expected differences in the UCL of c-UCNPs and css-UCNPs, the attachment of Cy3.5-ssDNA and unlabeled ssDNA on the UCNP surfaces via electrostatic interactions allowed us to investigate FRET for the different types of UCNPs at the different excitation modes (980 nm or 808 nm). Cy3.5-ssDNA dependent FRET-quenching of UCNP luminescence of up to ca. 20% was found for all UCNP–DNA conjugates. The use of both steady-state and time-resolved PL spectroscopy was necessary to conclude that the FRET-quenching was similar for the different UCNP–DNA conjugates (with c-UCNPs and css-UCNPs) and excitation conditions (with 980 nm and 808 nm). When comparing our results with other UCNP-to-dye energy transfer studies, which often revealed significant differences between steady-state and time-resolved PL results with quenching efficiencies below 50% in the most cases (Table 1), the determined quenching efficiency of ~20% seems realistic and the importance of a broad characterization (different types of UCNPs, different excitation wavelengths, both steady-state and time-resolved PL detection) becomes evident.

The higher sensitivity of the time-resolved setup and the concentration-independence of PL lifetimes provided us with a more precise picture of the energy transfer processes because

we were able to investigate rise and decay times of UCL as well as FRET-sensitized Cy3.5 PL. This time-resolved data showed that the longer donor–acceptor distances in css-UCNPs (in which the two shells separate the dye-acceptors further from the Er^{3+} donors in the core) were alleviated by the improved optical properties of the shell-protected donors and resulted in very similar FRET-quenching of UCL for all UCNP–DNA conjugates. The differences in UCL decay and rise times even for the same css-UCNPs but depending on the excitation wavelength (980 nm or 808 nm) also showed that excitation and de-activation (*via* emission or FRET) are closely related, most probably due to the different and multiple energy pathways and long-lived excited states in UCNPs.

While our results showed the importance of a detailed analysis of UCNP FRET under varying but comparable conditions and with both steady-state and time-resolved PL spectroscopy, we could also show that the time-gated FRET-sensitized Cy3.5 PL intensity could be used for quantifying DNA in water over approximately four orders of magnitude. Although this detection was independent of the type of UCNP or the mode of excitation, the brightest css-UCNP[λ_{ex} = 980 nm] provided the highest precision whereas the lower Cy3.5 PL intensities of css-UCNP[λ_{ex} = 808 nm] showed the necessity of optimizing Nd-excitation based UCNP-FRET. Nevertheless, this proof-of-concept for UCNP-FRET quantification of DNA by both 980 nm and 808 nm excitation is very encouraging for future studies toward applicable nucleic acid biosensors and our results demonstrated the importance of a profound and careful spectroscopic analysis of such UCNP–DNA nanohybrids.

Conflicts of interest

There are no conflicts to declare.

Acknowledgements

Notes and references

1 *FRET – Förster Resonance Energy Transfer*, ed. I. Medintz and N. Hildebrandt, John Wiley & Sons, 2013.

2 J. R. Lakowicz, *Principles of Fluorescence Spectroscopy*, Springer US, 2006.

3 O. Tagit and N. Hildebrandt, *ACS Sens.*, 2017, **2**, 31–45.

4 K. E. Sapsford, L. Berti and I. L. Medintz, *Angew. Chem., Int. Ed.*, 2006, **45**, 4562–4589.

5 A. C. S. Samia, X. Chen and C. Burda, *J. Am. Chem. Soc.*, 2003, **125**, 15736–15737.

6 D. Geißler and N. Hildebrandt, *Anal. Bioanal. Chem.*, 2016, **408**, 4475–4483.

7 M. Cardoso Dos Santos and N. Hildebrandt, *TrAC, Trends Anal. Chem.*, 2016, **84**, 60–71.

8 W. R. Algar, N. Hildebrandt, S. S. Vogel and I. L. Medintz, *Nat. Methods*, 2019, **16**, 815–829.

9 B. W. van der Meer, *FRET – Förster Reson. Energy Transf*, 2013.

10 N. Hildebrandt, in *FRET – Förster Resonance Energy Transfer*, Wiley-VCH Verlag GmbH & Co. KGaA, 2013, pp. 105–163.

11 C. Li, J. Zuo, Q. Li, Y. Chang, Y. Zhang, L. Tu, X. Liu, B. Xue, H. Zhao, H. Zhang and X. Kong, *Biosens. Bioelectron.*, 2017, **92**, 335–341.

12 S. Li, L. Xu, M. Sun, X. Wu, L. Liu, H. Kuang and C. Xu, *Adv. Mater.*, 2017, **29**, 1606086.

13 P. Jiang, M. He, L. Shen, A. Shi and Z. Liu, *Sens. Actuators, B*, 2017, **239**, 319–324.

14 S. F. Himmelstoß and T. Hirsch, *Methods Appl. Fluoresc.*, 2019, **7**, 22002.

15 B. del Rosal and D. Jaque, *Methods Appl. Fluoresc.*, 2019, **7**, 22001.

16 G. Jalani, V. Tam, F. Vetrone and M. Cerruti, *J. Am. Chem. Soc.*, 2018, **140**, 10923–10931.

17 B. Chen, Q. Su, W. Kong, Y. Wang, P. Shi and F. Wang, *J. Mater. Chem. B*, 2018, **6**, 2924–2944.

18 A. Gnach, T. Lipinski, A. Bednarkiewicz, J. Rybka and J. A. Capobianco, *Chem. Soc. Rev.*, 2015, **44**, 1561–1584.

19 H. Oliveira, A. Bednarkiewicz, A. Falk, E. Fröhlich, D. Lisjak, A. Prina-Mello, S. Resch, C. Schimpel, I. V. Vrček, E. Wysokińska and H. H. Gorris, *Adv. Healthcare Mater.*, 2019, **8**, 1801233.

20 Z. Zhang, S. Shikha, J. Liu, J. Zhang, Q. Mei and Y. Zhang, *Anal. Chem.*, 2019, **91**, 548–568.

21 C. Wang, X. Li and F. Zhang, *Analyst*, 2016, **141**, 3601–3620.

22 Y. Liu, X. Meng and W. Bu, *Coord. Chem. Rev.*, 2019, **379**, 82–98.

23 N. Hildebrandt, C. M. Spillmann, W. R. Algar, T. Pons, M. H. Stewart, E. Oh, K. Susumu, S. A. Díaz, J. B. Delehanty and I. L. Medintz, *Chem. Rev.*, 2017, **117**, 536–711.

24 C. Chen and N. Hildebrandt, *TrAC, Trends Anal. Chem.*, 2020, **123**, 115748.

25 P. A. Rojas-Gutierrez, S. Bhuckory, C. Mingoes, N. Hildebrandt, C. DeWolf and J. A. Capobianco, *ACS Appl. Nano Mater.*, 2018, **1**, 5345–5354.

26 L. Francés-Soriano, M. Liras, A. Kowalczyk, A. Bednarkiewicz, M. González-Béjar and J. Pérez-Prieto, *Nanoscale*, 2016, **8**, 204–208.

27 K. Liu, X. Liu, Q. Zeng, Y. Zhang, L. Tu, T. Liu, X. Kong, Y. Wang, F. Cao, S. A. G. Lambrechts, M. C. G. Aalders and H. Zhang, *ACS Nano*, 2012, **6**, 4054–4062.

28 V. Muhr, C. Würth, M. Kraft, M. Buchner, A. J. Baeumner, U. Resch-Genger and T. Hirsch, *Anal. Chem.*, 2017, **89**, 4868–4874.

29 O. Dukhno, F. Przybilla, M. Collot, A. Klymchenko, V. Pivovarenko, M. Buchner, V. Muhr, T. Hirsch and Y. Mély, *Nanoscale*, 2017, **9**, 11994–12004.

30 S. Bhuckory, E. Hemmer, Y. T. Wu, A. Yahia-Ammar, F. Vetrone and N. Hildebrandt, *Eur. J. Inorg. Chem.*, 2017, **2017**, 5186–5195.

31 Y. Wang, K. Liu, X. Liu, K. Dohnalová, T. Gregorkiewicz, X. Kong, M. C. G. Aalders, W. J. Buma and H. Zhang, *J. Phys. Chem. Lett.*, 2011, **2**, 2083–2088.

32 S. Lahtinen, Q. Wang and T. Soukka, *Anal. Chem.*, 2016, **88**, 653–658.

33 L. Mattsson, K. D. Wegner, N. Hildebrandt and T. Soukka, *RSC Adv.*, 2015, **5**, 13270–13277.

34 M. González-Béjar, M. Liras, L. Francés-Soriano, V. Voliani, V. Herranz-Pérez, M. Duran-Moreno, J. M. Garcia-Verdugo, E. I. Alarcon, J. C. Scaiano and J. Pérez-Prieto, *J. Mater. Chem. B*, 2014, **2**, 4554–4563.

35 L. Francés-Soriano, S. Gonzalez-Carrero, E. Navarro-Raga, R. E. Galian, M. González-Béjar and J. Pérez-Prieto, *Adv. Funct. Mater.*, 2016, **26**, 5131–5138.

36 B. Liu, C. Li, P. Yang, Z. Hou and J. Lin, *Adv. Mater.*, 2017, **29**, 1605434.

37 M. J. Weber, *Phys. Rev. B: Solid State*, 1971, **4**, 3153–3159.

38 M.-H. Chan and R.-S. Liu, *Nanoscale*, 2017, **9**, 18153–18168.

39 S. T. Dibaba, X. Ge, W. Ren and L. Sun, *J. Rare Earths*, 2019, **37**, 791–805.

40 Y. Zhang, Z. Yu, J. Li, Y. Ao, J. Xue, Z. Zeng, X. Yang and T. T. Y. Tan, *ACS Nano*, 2017, **11**, 2846–2857.

41 F. Ai, Q. Ju, X. Zhang, X. Chen, F. Wang and G. Zhu, *Sci. Rep.*, 2015, **5**, 10785.

42 Z. Hou, K. Deng, C. Li, X. Deng, H. Lian, Z. Cheng, D. Jin and J. Lin, *Biomaterials*, 2016, **101**, 32–46.

43 M. S. Meijer, V. S. Talens, M. F. Hilbers, R. E. Kieltyka, A. M. Brouwer, M. M. Natile and S. Bonnet, *Langmuir*, 2019, **35**, 12079–12090.

44 N. J. J. Johnson, A. Korinek, C. Dong and F. C. J. M. van Veggel, *J. Am. Chem. Soc.*, 2012, **134**, 11068–11071.

45 N. J. J. Johnson, S. He, S. Diao, E. M. Chan, H. Dai and A. Almutairi, *J. Am. Chem. Soc.*, 2017, **139**, 3275–3282.

46 X. Xie, N. Gao, R. Deng, Q. Sun, Q.-H. Xu and X. Liu, *J. Am. Chem. Soc.*, 2013, **135**, 12608–12611.

47 F. He, C. Li, X. Zhang, Y. Chen, X. Deng, B. Liu, Z. Hou, S. Huang, D. Jin and J. Lin, *Dalton Trans.*, 2016, **45**, 1708–1716.

48 Y. Zhong, G. Tian, Z. Gu, Y. Yang, L. Gu, Y. Zhao, Y. Ma and J. Yao, *Adv. Mater.*, 2014, **26**, 2831–2837.

49 L. M. Wiesholler, F. Frenzel, B. Grauel, C. Würth, U. Resch-Genger and T. Hirsch, *Nanoscale*, 2019, **11**, 13440–13449.

50 S. Wilhelm, M. Kaiser, C. Würth, J. Heiland, C. Carrillo-Carrion, V. Muhr, O. S. Wolfbeis, W. J. Parak, U. Resch-Genger and T. Hirsch, *Nanoscale*, 2015, **7**, 1403–1410.

51 A. Dong, X. Ye, J. Chen, Y. Kang, T. Gordon, J. M. Kikkawa and C. B. Murray, *J. Am. Chem. Soc.*, 2011, **133**, 998–1006.

52 J. Guo, X. Qiu, C. Mingoes, J. R. Deschamps, K. Susumu, I. L. Medintz and N. Hildebrandt, *ACS Nano*, 2019, **13**, 505–514.

53 M. Y. Hossan, A. Hor, Q. Luu, S. J. Smith, P. S. May and M. T. Berry, *J. Phys. Chem. C*, 2017, **121**, 16592–16606.

54 C. Chen, B. Corry, L. Huang and N. Hildebrandt, *J. Am. Chem. Soc.*, 2019, **141**, 11123–11141.

55 P. D. M. Sauer, D. J. Enderlein and J. Hofkens, *Handbook of Fluorescence Spectroscopy and Imaging: From Single Molecules to Ensembles*, Wiley-VCH, 2011.

56 N. G. Zhegalova, S. He, H. Zhou, D. M. Kim and M. Y. Berezin, *Contrast Media Mol. Imaging*, 2014, **9**, 355–362.

57 J. Kang, O. Kaczmarek, J. Liebscher and L. Dähne, *Int. J. Polym. Sci.*, 2010, **2010**, 7.

58 L. Francés-Soriano, M. A. Zakharko, M. González-Béjar, P. A. Panchenko, V. Herranz-Pérez, D. A. Pritmov, M. A. Grin, A. F. Mironov, J. M. García-Verdugo, O. A. Fedorova and J. Pérez-Prieto, *Chem. Mater.*, 2018, **30**, 3677–3682.

59 A. L. De Guereñu, P. Bastian, P. Wessig, L. John and M. U. Kumke, *Biosensors*, 2019, **9**, 9.

60 Y. Ding, F. Wu, Y. Zhang, X. Liu, E. M. L. D. De Jong, T. Gregorkiewicz, X. Hong, Y. Liu, M. C. G. Aalders, W. J. Buma and H. Zhang, *J. Phys. Chem. Lett.*, 2015, **6**, 2518–2523.